Chapter 11

Enhancement of Cathodic H_2 Production Efficiencies by Simultaneous Anodic Oxidation of Organics: Role of Substrate and Active Chlorine Species

Sections reprinted with permission from Park, H.; Vecitis, C. D.; Hoffmann, M. R. J*ournal of Physical Chemistry A* **2009**, *113*.

Abstract

The need for alternative energy sources with minimal-to-no carbon footprint is growing. A solar-powered electrochemical system which produces hydrogen via water splitting using organic pollutants as sacrificial electron donors is a possible solution. The hybridization of a BiO_x-TiO_2/Ti anode with a stainless-steel cathode powered by a photo-voltaic (PV) array has been shown to achieve this process. The electrochemical degradation kinetics of a variety of organic substrates is investigated as a function of a background electrolyte NaCl vs. Na_2SO_4. The observed substrate (S) degradation kinetics ($-k_{obs}^{S}$) are found to correlate well with the cell current (I_{cell}) and the H_2 production energy efficiency (EE) in the presence of NaCl as the background electrolyte. In the case of Na_2SO_4, no correlation is observed and the degradation rates are greatly reduced in comparison to NaCl. This suggests the primary chemical oxidant is electrolyte-dependent. $-k_{obs}^{S}$s are found to be proportional to bimolecular rate constants of $Cl_2^{\bullet-}$ with the substrate ($k_{Cl_2^{\bullet-}+S}$) and to substrate-induced ΔEEs (EE with substrate – EE without substrate) in the presence of NaCl. The ΔEE correlation arises from the active chlorine species acting as an electron shuttle, which compete with H_2 production for cathodic electrons. In the presence of the organic substrates, the active chlorine species are quenched, increasing the fraction of electrons utilized for the H_2 production.

Introduction

As the cost of fossil fuels increases, the development of alternative, renewable, and environmentally benign (i.e., carbon-free) sources of energy is paramount[1,2]. Hydrogen, as a potential alternative fuel, has a higher energy density (per kg) than gasoline or alcohols and a viable storage capacity under high pressures. Electrochemical water splitting (i.e., electrolysis) for H_2 generation has a negligible carbon footprint compared to steam methane reformation (SMR), which is the predominant H_2 production method today. At present, commercial-scale water electrolyzer efficiencies range from 50 to 75% efficient[3–5]. yet the cost of electrolytic hydrogen production technology is continuing to rise because of rising electricity costs. In order to lower the cost of electrolytic H_2 production, it may prove beneficial to couple electrochemical water treatment with hydrogen generation. The hybridization of these two processes should result in a single, cooperative, and more cost-effective electrochemical process. Conventional water and wastewater treatment operations are known to be energy-intensive and correspond to > 20% of local energy expenditures for water-scarce municipalities[6].

Solar-powered electrolytic systems have been developed to couple hydrogen production with the simultaneous remediation of environmentally relevant organic pollutants[7,8]. In these systems, a photovoltaic (PV) cell is used to convert solar light into DC current, which in turn powers the electrochemical cell. At a multi-component, hetero-junction anode, organic compounds are converted primarily to carbon dioxide and lower-molecular-weight organic acids. At a stainless-steel (SS) cathode, hydrogen is produced via water or proton reduction. Anodic oxygen evolution (i.e., water oxidation) is circumvented by the generation of oxidizing radical species resulting in a non-

stoichiometric water splitting (i.e., overall H_2/O_2 mole ratios of 6 to 8). Anodic current efficiencies for the one-electron oxidation and for the complete mineralization of phenol range from 7 to 17% and 3 to 10%, respectively. The cathodic current and energy efficiencies for hydrogen generation range from 50 to 70% and 30 to 60%, respectively.

In addition, the oxidation of organics substrates (e.g., phenol) appears to increase 1) the rate of H_2 production, 2) the H_2 production energy efficiency by 50%, and 3) the cell voltage (E_{cell}) by 0.1–0.2 V in the photovoltaic (PV)-connected system[7,8]. The relative degree of the apparent "substrate-induced synergy effect" is dependent on the supporting electrolyte. For example, sodium chloride has a large efficiency enhancement effect, whereas sodium sulfate has minimal effect. In addition, the degradation rate of phenol in sodium chloride is faster by more than two orders of magnitude than that in sodium sulfate.

Sodium chloride is often utilized as a supporting electrolyte in electrochemical water treatment[9–23] NaCl improves .e anodic oxidation efficiency for phenol[10,11,13,15,16], glucose[12,17], p-cresol[9], propylene glycol[22], trichlosan[14], oxalic acid[18], dyestuffs[20,21], and endocrine disruptors[23], compared to sodium sulfate[10,12,23], sodium bicarbonate[9], and sodium nitrate[23]. In some cases, chlorinated substrates enhance anodic efficiencies due to the liberation of chlorine during the course of electrolysis[24]. Active chlorine species such as $Cl^{\bullet}$, $Cl_2^{\bullet-}$, and ClO^- are generated at the anode surface and act as indirect oxidants for organic or inorganic reductants. However, the impact of reactive chlorine intermediates on cathodic reactions has not been studied in detail (e.g., the impact of reaction chlorine species on hydrogen production rates in this study). With this in mind, we have compared a variety of substrates in terms of relative anodic oxidation efficiencies and the

corresponding effects on cathodic hydrogen production using NaCl or Na_2SO_4 as the supporting electrolytes.

Experimental Details

Chemical Reagents

All chemicals were reagent or HPLC grade. Phenol (PhOH, J.T.Baker), catechol (CC, Sigma), hydroquinone (HQ, J.T.Baker), 2-chlorophenol (2CP, Aldrich), 4-chlorophenol (4CP, Aldrich), 2,4-dichlorophenol (24CP, TCI), 2,6-dichlorophenol (26CP, TCI), 2,4,6-trichlorophenol (246CP, TCI), salicylic acid (SA, Aldrich), benzoic acid (BA, J.T.Baker), methanol (EMD), sodium formate (Aldrich), sodium acetate (Aldrich), maleic acid (Sigma), malonic acid (Sigma), sodium oxalate (Aldrich), and sodium hypochlorite (NaOCl, VWR) were used as received. NaCl (J.T.Baker), Na_2SO_4 (EMD), or CO_2(g)-purged $NaHCO_3$ was used as a supporting electrolyte.

Electrodes

A BiO_x-TiO_2-Ti(0) electrode was used as the primary anode. Details of the anode preparation are provided elsewhere[7,8,22]. In summary, the electrode consists of a series of metal oxide coatings on a titanium metal substrate. They include a pre-coating, sealing coating, slurry coating, and over-coating. Each step of coating requires a specific heat treatment regime with different temperatures and times. A single thin anode with an active area of 25.5 cm^2 and two stainless-steel (SS) cathodes (Hastelloy C-22) of equal size were used as the electrodes. A cathode was placed on both sides of the double-sided anode with a separation distance of 2 mm.

Electrolytic Reactions

The double-sided BiO_x-TiO_2-Ti(0) anode coupled with SS cathodes was immersed in aqueous electrolyte solutions of either sodium chloride or sodium sulfate (200 mL). The electrolyte solution was stirred during continuous purging with air or nitrogen as a background carrier gas. The target substrates were added to the background electrolyte at t = 0 or added subsequently during the course of electrolysis. A constant cell voltage or current was applied to the electrodes with a DC-power supply (HP 6263B and 6260B). The current efficiencies (eq. 11.1) and the energy efficiencies (eq. 11.2) were obtained using the following equations.

$$\text{Current efficiency (\%)} = \frac{\text{Number of molecules produced } (H_2, O_2, \text{ or } CO_2) \text{ or degraded (phenol)}}{\text{Number of electrons flowed}} \times n \times 100 \quad (11.1)$$

where n = 2 and 4 for cathodic hydrogen and anodic oxygen production, respectively. For anodic current efficiencies, n = 1 for one-electron oxidation of phenol, and n = 14/3 for the complete oxidation of phenol carbon to carbon-dioxide carbon.

$$H_2 \text{ energy efficiency (\%)} = \frac{(39 W \cdot h/g \times H_2 \text{ rate} \times 2 g/mol)}{E_{cell} \times I_{cell}} \times 100 \quad (11.2)$$

Chemical Analyses

The electrolytic reactor was sealed to the atmosphere. The gas in the headspace was extracted using a peristaltic pump and pushed through a membrane inlet and then pulled into a mass spectrometer (MS) under a vacuum (5.0×10^{-6} torr) generated with a turbo pump (Pfeiffer). The extracted gases were ionized by 70 eV electron impact and subsequently analyzed by quadrupole mass spectrometry (Balzers). The volume percent of the headspace was calculated assuming that it was directly proportional to the ion

current measured by the mass spectrometer (i.e., the transfer of all gases through the membrane and their 70 eV electron ionization cross-sections were approximately equivalent). This assumption was validated by the fact that ambient air was determined to be 77% nitrogen, 17% oxygen, 5% water vapor, and 1% argon.

Aromatic compounds and their reaction intermediates were analyzed by a high-performance liquid chromatography (HPLC, Agilent 1100 series) using a C18 column for separation. The eluent was composed of 55% Milli-Q water (0.1 wt% acetic acid) and 45% acetonitrile at flow rate of 0.7 mL/min.

Results and Discussion

Substrate-Specific Reaction Rates

A time profile of H_2 and O_2 production at the BiO_x-TiO_2-Ti(0)/SS electrode couple is shown in Figure 11.1 for a background electrolyte concentration of 50 mM NaCl. In the absence of phenol (i.e., conventional water electrolysis), the initial H_2 production rate was observed to range from 90 to 100 μmol min^{-1}. Under steady-state conditions, however, the H_2 production rate declined slightly to 80 μmol min^{-1}. In contrast, with the addition of phenol to the reaction mixture, the H_2 production rate increased again to 110 μmol min^{-1}. The apparent substrate enhancement of the H_2 production rate is maintained for a short period after the incremental addition of phenol, and then it relaxes back to the state-state condition as the rate of CO_2 production is maximized. On the other hand, the addition of an oxidizable substrate has little impact on the rate of O_2 production.

Other phenolic substrates—such as catechol, hydroquinone, salicylic acid, 2-chlorophenol, and 4-chloropenol—exhibit similar behavior as shown in Figure 11.2a, whereas maleic acid, malonic acid, and oxalic acid have a lesser rate enhancement than

the phenolic substrates. Lower molecular weight compounds such as methanol, formate, and acetate do not show any synergistic effects on the hydrogen production rates.

The addition of phenol to the electrolytic system lowers the cell current from 0.38 A to 0.32 A under a constant DC cell voltage of 3.1 V in spite of an increase in hydrogen production by 20 μmol min^{-1} (Table 11.1). Maleic acid, oxalic acid, catechol, salicylic acid, and the chlorinated phenols also increase the hydrogen production efficiency, while concurrently lowering cell current. When the electrolytic cell is powered by a PV array, then the cell voltage is increased from 4.0 V to 4.2 V upon addition of phenol, while the cell current remains constant[7]. Therefore, the substrate synergistic effect on the hydrogen production energy efficiency is twofold: the hydrogen production rates are increased and the cell currents are decreased at a constant DC cell voltage. The addition of aromatic substrates results in an increase in the apparent energy efficiencies by 30 to 50%, whereas the addition of maleic or oxalic acid increases the efficiencies by only 8 to 10% (Table 11.1).

The degradation of the phenolic substrates follows pseudo-first-order kinetics. The observed reaction rate constants ($-k_{obs}^{S}$) appear to be dependent on the chemical structure under similar electrolytic conditions (I_{cell} = 0.375A; 50 mM NaCl).

$$\frac{d[S]}{dt} = -k_{obs}^{S}[S] \tag{11.3}$$

For example, the degradation rates of hydroquinone and 2,4,6-trichlorophenol are 4.6 and 3.7 times faster than phenol, respectively (Figure 11.2b & Table 11.1). On the other hand, the degradation rates of salicylic acid and benzoic acid are 2 and 250 times slower than phenol, respectively. It appears that the presence of a aromatic ring substituent such as a

chlorine (-Cl) and/or hydroxyl group (-OH) enhances the apparent degradation rates, while carboxyl groups (-COOH/-COO^-) decrease the observed rates relative to phenol[25,26].

NaCl and $NaSO_4$ as Background Electrolytes

To investigate the nature of the substrate-induced synergistic effects, sodium sulfate was used as the electrolyte and compared with sodium chloride in terms of the electrochemical hydrogen production and substrate degradation rates. The hydrogen production energy efficiencies in the sodium sulfate range from 50 to 80%, depending on the applied power. The efficiencies are 10 to 20% higher than those observed for sodium chloride (Figure 11.3a). However, upon addition of phenol to the sodium sulfate electrolyte, the hydrogen production rate decreases slightly with no apparent synergy (Figure 11.3b). The electrolytic degradation rates of phenol, salicylic acid, and benzoic acid with Na_2SO_4 as the background electrolyte are lower than those with a NaCl electrolyte system (Figure 11.3c vs. Figure 11.2b; Table 11.1). For example, the degradation rate of *0.1 mM* phenol in sodium sulfate is 37 times lower than that of *1 mM* phenol in sodium chloride ($-k_{obs}^{PhOH}$ (in NaCl) / $-k_{obs}^{PhOH}$ (in Na_2SO_4) = 37) (implying the degradation rate of 1 mM phenol in sodium sulfate should be much lower). The degradation of salicylic acid also shows a similar rate difference, e.g., $-k_{obs}^{SA}$ (in NaCl) / $-k_{obs}^{SA}$ (in Na_2SO_4) = 19. However, the variation of the observed degradation rates with structure of the organic substrates is substantially less in Na_2SO_4 than NaCl (e.g., $-k_{obs}^{SA} / -k_{obs}^{PhOH}$ = 0.41 and $-k_{obs}^{BA} / -k_{obs}^{PhOH}$ = 0.0045 in NaCl; $-k_{obs}^{SA} / -k_{obs}^{PhOH}$ = 0.81 and $-k_{obs}^{BA} / -k_{obs}^{PhOH}$ = 0.13 in Na_2SO_4). These results suggest that the primary oxidant (e.g., $SO_4\cdot^-$, ·OH radical or surface bound holes, h^+) in the Na_2SO_4 electrolytic system is of lower concentration and/or less discriminating in terms of likely reaction sites.

A change in the supporting electrolyte also affects the extent of pH change during the course of electrolysis. After initiation of electrolysis in a pure sodium chloride solution, the pH immediately rises from 6 to 10, and then is maintained at a steady state throughout continued electrolysis (Figure 11.4a)[8]. After terminating the electrolysis, the pH decreases to 9.5. However, in the presence of phenol, the pH increases to 11 during the initial stages of electrolysis and subsequently declines to a value below pH 7 as small organic acids are produced. Upon continued electrolysis, the pH increases slightly to circum-neutral range (~ pH 7.5). Electrolytic hydrogen production consumes protons and/or generates hydroxide ions resulting in increase of pH. However, continued oxidation of phenol results in the formation of ring-opening intermediates leading to the production of short-chained organic acids such as oxalic acid and maleic acid, which may serve to lower the pH.

The pH vs. time profile during the electrolysis of pure sodium sulfate is similar to that observed in pure NaCl electrolyte. On the other hand, the pH vs. time profile during the electrolytic oxidation of phenol in a background sodium sulfate electrolyte (Na_2SO_4 + phenol) is clearly different than that observed during electrolysis in Na_2SO_4 alone. In addition, the pH vs. time profile for Na_2SO_4 electrolysis has a different shape than that observed in the case of the electrolytic oxidation of phenol in the presence of sodium chloride electrolyte. In particular, the pH does not return to the circum-neutral range at any time during the electrolysis. The degradation rates of substrates during sodium sulfate electrolysis are much slower than those in the sodium chloride (Figure 11.2b vs. 11.3c; Table 11.1). The apparent pH-lowering effect during NaCl electrolysis is due to the production of the short-chained organic acids. However, in the case of Na_2SO_4

electrolytic phenol oxidation, the short-chain carboxylates are either not electrolysis intermediates or not produced on the timescale of the current electrolysis experiments. This is consistent with the observation that CO_2 is not produced during the course of phenol electrolysis in the presence of sodium sulfate.

Primary Reactive Intermediate Species

The presence of titanol groups (i.e., >TiOH) on the hydrated, anodic TiO_2 surface implies that the initiation of the oxidation proceeds via formation of either a surface-bound hydroxyl radical (>Ti-OH$^{\bullet}$) or a free hydroxyl radical ($^{\bullet}$OH) (A1 in Table 11.2). The initiation of the cathodic reaction proceeds via the one electron-reduction of dissolved oxygen molecules (A7 and E1), protons, or water (E2). However, further reactions may have many parallel or sequential steps in which the supporting electrolyte is either directly or indirectly involved the subsequent reactions. For example, the electrochemical oxidation of organic substrates in the presence of a sodium chloride electrolyte has six or more possible oxidation pathways. They include direct electron transfer from the substrate to surface-bound OH$^{\bullet}$, and indirect homogeneous reactions with free OH$^{\bullet}$, Cl$^{\bullet}$, $Cl_2^{\bullet-}$, HClO/ClO^-, and H_2O_2 (Table 11.2).

>TiOH$^{\bullet}$/OH$^{\bullet}$

Figures 11.5a and b show the correlation between the normalized pseudo-first-order electrolysis rates for the substrates ($k^{o}_{obs} = - k^{S}_{obs} / - k^{PhOH}_{obs}$) and the relative bimolecular reaction rate constants of $^{\bullet}$OH and $Cl_2^{\bullet-}$ with respect to phenol ($k^{o}_{OH} = k_{OH+S} / k_{OH+PhOH}$; $k^{o}_{Cl_2^-} = k_{Cl_2^-+S} / k_{Cl_2^-+PhOH}$)[27–29]. The k^{o}_{obs} vs. k^{o}_{OH} data are not correlated. This suggests that hydroxyl radicals are not the primary oxidant involved in the anodic reactions. The steady-state concentration of OH radicals (i.e., [$^{\bullet}$OH] = [>Ti-OH$^{\bullet}$] + [free $^{\bullet}$OH]) can be

estimated assuming that 20% of applied current generates oxygen (i.e., $I_{an}^{O_2} = 0.2I_{an}$) and the reaction of OH radical with Cl^- is the dominant $OH^\bullet$ pathway ($k_{OH+Cl^-}[Cl^-] >> k_{OH+ClO^-}[ClO^-] + k_{OH+S}[S]$). The assumption of $I_{an}^{O_2} / I_{an} = 0.2$ is valid, since typical H_2/O_2 ratio is approximately 7 and the cathodic hydrogen production current efficiency is 70% (i.e., $H_2/O_2 = 7$; $I_{cell} = I_{an} = I_{ca}$; $I_{ca}^{H_2} / I_{ca} = 0.7$; $I_{an}^{O_2} = 2 \times I_{ca}^{H_2}$, thus $I_{an}^{O_2} / I_{an} = 0.2$).

$$\frac{d[OH^\bullet]}{dt} = \frac{4I_{an} - I_{an}^{O_2}}{4FV} - (k_{OH+Cl^-}[Cl^-] + k_{OH+ClO^-}[ClO^-] + k_{OH+S}[S])[OH^\bullet] \quad (11.4)$$

$$[OH^\bullet]_{SS} = \frac{4I_{an} - I_{an}^{O_2}}{4FV(k_{OH+Cl^-}[Cl^-]_{SS})} \quad (11.5)$$

At I_{cell} = 0.375A and in the presence of 50 mM NaCl, the steady-state hydroxyl radical concentration is estimated to be 1.6×10^{-15} mol cm^{-2} at the anode surface (corresponding to 8.6×10^{-15} mol L^{-1} if all $OH^\bullet$ were released to solution). This number is seven orders of magnitude smaller than the typical site density of >Ti-OH groups on colloidal TiO_2 (i.e., assuming 5 hydroxy sites nm^{-2}), which is equivalent to 1×10^{-8} mol-OH cm^{-2} [30]. Thus, once produced, the surface-bound or free hydroxyl radical immediately reacts with chloride ion to yield $Cl^\bullet$. The low >TiOH$^\bullet$ concentration also yields a large number of potential binding sites for a substrate sorption to the TiO_2 surface and direct electron transfer reactions may occur simultaneously with homogeneous oxidations.

$Cl^\bullet$

The possible active chlorine species include $Cl^\bullet$, $Cl_2^{\bullet-}$, HClO, and ClO^-. In aqueous solution, the active chlorine species will be in equilibrium with each other and their redox

potentials are as follows: $E°(Cl^{\bullet}/Cl^{-}) > E°(Cl_2^{\bullet-}/2Cl^{-}) > E°(HClO/0.5Cl_2) > E°(Cl^{-}/HClO) > E°(Cl^{-}/ClO^{-})$ (D1–D3)[31]. From a thermo-chemical perspective, $Cl^{\bullet}$ is the most reactive species towards one electron oxidation. It has a similar reactivity when compared to $^{\bullet}OH$ radical ($E°(OH^{\bullet}/H_2O) = 2.7$ V)[29]. And the $Cl^{\bullet}$ second-order rate constants for reaction with a wide range of aliphatic organic compounds (RH) are well correlated (k_{OH+RH} vs. k_{Cl+RH}).[32] $Cl^{\bullet}$ readily undergoes rapid addition, hydrogen-abstraction, and direct electron transfer reactions with aromatics at second-order rate constants ranging from 10^8 to 10^9 M^{-1} s^{-1}. $Cl^{\bullet}$ is generated through a transient adduct of Cl^{-} with the $>Ti\text{-}OH^{\bullet}$ group at the anode surface, or by direct hole oxidation of $>TiOHCl^{-}$ surface groups and subsequent protonation of the adduct (A4). Assuming all reactions are diffusion controlled, the $Cl^{\bullet}$ branching ratio depends on the Cl^{-} concentration relative to S concentration; at low $[Cl^{-}]/[S] < 1$, the reaction of $Cl^{\bullet}$ with substrates is predominant, whereas at high $[Cl^{-}]/[S] > 1$ concentration, $Cl_2^{\bullet-}$ formation should occur preferentially[32,33]. The relatively high Cl^{-} concentration (50 mM) as compared to substrates (~ 1 mM) in our system pushes $Cl^{\bullet}$ branching towards $Cl_2^{\bullet-}$ formation. The nondetection of $Cl_{2(g)}$ is consistent with $Cl_2^{\bullet-}$ formation (i.e., B3 and B5 are negligible).

$Cl_2^{\bullet-}$

At high background chloride concentrations, $[Cl^{-}]/[S] > 1$, $Cl_2^{\bullet-}$ should dominate the active chlorine species. When k^{o}_{obs} values are plotted against known $k^{o}_{Cl_2^{\bullet-}+S}$ values for phenol, salicylic acid, hydroquinone, and benzoic acid, an excellent linear correlation is obtained ($R^2 > 0.99$), as shown in Figure 11.5b. This strongly indicates that the dichloride radical anion is a primary oxidant species during electrolysis with sodium chloride. The

dichloride radical anion is in equilibrium with $Cl^{\bullet}$ and Cl^{-} (B4: $K_{eq} = 1.4\times10^{5}$ M^{-1}; $[Cl^{-}] =$ 50 mM, $[Cl_2^{\bullet-}]/[Cl^{\bullet}] = 7\times10^{3}$) and the forward reaction is diffusion controlled[28,34,35]. Like $Cl^{\bullet}$, $Cl_2^{\bullet-}$ reacts with organics via hydrogen abstraction, electrophilic addition, and direct electron transfer mechanisms. However, $Cl_2^{\bullet-}$ bimolecular oxidation kinetics is typically two to four orders of magnitude slower than $Cl^{\bullet}$. $Cl_2^{\bullet-}$ reacts with the aliphatic compounds primarily through a hydrogen abstraction mechanism with rate constants ranging from $< 10^{3}$ to 10^{6} M^{-1} s^{-1} [36,37]. The H-abstraction rates are controlled by the C-H bond dissociation energy. In addition, deprotonated substrates are less reactive than their protonated counterparts. For example, the reaction rate of $Cl_2^{\bullet-}$ with formic acid is two to three orders of magnitude greater than with formate (Table 11.1), consistent with H-abstraction being the predominant mechanism. $Cl_2^{\bullet-}$ oxidation mechanisms and kinetics are also affected by size (i.e., steric hindrance) and electron donating/withdrawing character of aromatic substituents.

The reaction of $Cl_2^{\bullet-}$ with aromatic compounds involves H-atom abstraction, direct electron transfer or electrophilic addition, with rate constants ranging from 10^{6} to 10^{9} $M^{-1}s^{-1}$. A previously reported Hammett plot of para-substituted phenols indicates that electron-withdrawing substituents such as -COOH and -CN decrease the rate relative to phenol, whereas electron-donating substituents such as $-OCH_3$, $-COO^{-}$, and -OH, increase the rate relative to phenol[36]. The results suggest an electrophilic addition or direct electron transfer mechanism, which would benefit from increased electron density, are active. Figure 11.5d shows a plot between k^{o}_{obs} and the corresponding Hammett (σ) constants. The observed V behavior suggests $Cl_2^{\bullet-}$ oxidation has two branching pathways[38,39]. The negative correlation ($-0.4 < \sigma < 0.2$, $R^2 > 0.93$) is in agreement with

previous pulse radiolysis results, suggesting a Cl-addition or direct electron transfer pathway. Once $\sigma > 0.2$, k^{o}_{obs} is positively correlated with σ, indicating a change in the $Cl_2^{\bullet-}$ oxidation mechanism. The addition of bulky Cl-subtituents may sterically hinder $Cl_2^{\bullet-}$ from an intimate encounter with the phenol retarding a Cl-addition or direct electron transfer pathway. Steric hindrance could explain why Cl-addition/electron transfer is no longer the primary pathway, but can not explain the rate increase. The subsequent addition of electron withdrawing groups removes electron density from the ring and weakens the remaining Ar-H bonds. $Cl_2^{\bullet-}$ H-abstraction rates with aliphatics are directly proportional to the C-H bond strength. This would suggest a $Cl_2^{\bullet-}$ H-abstraction mechanism is present in the positive correlation regime. Another plausible explanation is that the increased electron-withdrawing character will reduce the pK_a and a shift in branching pathway is the result of aqueous speciation (i.e, phenol vs. phenoxide).

HOCl/OCl$^-$

Hypochlorous acid (HOCl) or hypochlorite (ClO^-) can be electrochemically produced via a number of mechanisms: direct hole oxidation of >Ti-$OHCl^{\bullet-}$ at the anode surface (A5), $Cl_2^{\bullet-}$-oxidation of H_2O (B7), or by reaction of $Cl_2^{\bullet-}$ and >Ti-$OH^{\bullet}$/$OH^{\bullet}$ (here no distinction between surface-bound and free OH radical) (B8). Many investigators argue that hypochlorous acid (E° = 1.63V) and hypochlorite ion (E° = 0.90V) are the primary oxidants in the electrochemical degradation of organics in a sodium chloride medium[9,10,12,18,24]. In this study, the production of hypochlorite was only observed during the electrolysis of NaCl in the absence of organics (Figure 11.6a). During NaCl electrolysis, hypochlorite increases in concentration reaching a plateau of 5 mM after 1 h of electrolysis. Absence of $HOCl/OCl^-$ accumulation in the presence of phenol would

suggest a HOCl/OCl^- loss mechanism via substrate oxidation. However, as shown in Figure 11.5c there is no correlation between the normalized electrochemical oxidation rates (k^{o}_{obs}) and the normalized bimolecular rate constants of HOCl with substrates (k^{o}_{HOCl}). Additionally, HOCl has relatively slow second-order rate constants with phenol (e.g., $k_{HOCl+PhOH} = 2.19 \times 10^4$ M^{-1} s^{-1} and $k_{Cl_2^{\bullet-}+PhOH}/k_{HOCl+PhOH} = 1.14 \times 10^5$) and becomes even slower with OH- or Cl-addition (i.e., 10^1 to 10^3 M^{-1} s^{-1}, $k_{Cl_2^{\bullet-}+HQ}/k_{HOCl+HQ} = 3.11 \times 10^6$)[40]. An alternative mechanism is proposed by examining the pathways for HOCl production which involve $Cl_2^{\bullet-}$ as an intermediate (B7, B8). Substrate addition will consume $Cl_2^{\bullet-}$ subsequently inhibiting the HOCl production pathways. The alternative mechanism HOCl inhibition through intermediate $Cl_2^{\bullet-}$ consumption is consistent with kinetic correlations and time-dependent HOCl observation.

The effect of the hypochlorite on electrochemistry was investigated by spiking the reactor to 5 mM NaOCl during electrolysis of 50 mM NaCl at a constant cell voltage (E_{cell} = 3.17 V, Figure 11.6b). Immediately after addition, the hydrogen production rate decreased, then slowly recovered and eventually exceeded the initial production rate. The oxygen production rate increased upon NaOCl addition and retained a higher production rate during continued electrolysis. The addition of sodium hypochlorite also increased the cell current from 0.38 A to 0.44 A. A subsequent NaOCl addition yielded similar results (i.e, the cell current increases again from 0.43 A to 0.50 A). After continued electrolysis, a slight decrease in cell current is observed (e.g., 0.44 A to 0.43 A; 0.50 A to 0.48 A).

Cl^IO^- can be electrochemically oxidized to chlorate ion ($Cl^VO_3^-$) with simultaneous generation of oxygen (B20) or reduced to chloride ion (D3). The oxidative pathway (B20)

increases the overall oxygen production, while the reductive pathway (D3) competitively reduces the hydrogen production (E2) leading to initial decrease of the hydrogen production rate. The oxidative pathway (B20) yields a greater electron flow through the circuit and increases the cell current and the hydrogen production rate as the electrolysis proceeds. It was reported that chlorate anion (ClO_3^-) is produced either when hypochlorous acid is hydrolyzed (B20)[12] or when Cl_2 gas is released at a boron-doped diamond electrode[41].

H_2O_2

Hydrogen peroxide (H_2O_2) can be produced by an anodic surface recombination pathway (A3), through hydroxyl radical recombination (B8), or hydroperoxy radical recombination (A7c). The oxidation of substrates such as phenol with NaCl as an electrolyte does not produce any hydroxylated intermediates (e.g., catechol, hydroquinone, resorcinol); instead, only chlorinated phenols such as 2-/4-chlorophenol, 2,4-/2,6-dichlorophenol, and 2,4,6-trichlorophenol were observed as intermediates[7,8]. This suggests that even if hydrogen peroxide is produced, it contributes little to the oxidation of the substrates. Hydrogen peroxide can be oxidized by the hydroxyl radical (B9, $k = 2.7 \times 10^7\ M^{-1}\ s^{-1}$) or $Cl_2^{\bullet-}$ (B12, $k = 1.4 \times 10^5\ M^{-1}\ s^{-1}$) to hydroperoxyl radical ($HOO^{\bullet}$), which is further oxidized by $Cl_2^{\bullet-}$ to oxygen (B13) at diffusion-limited rates ($k = 3 \times 10^9\ M^{-1}\ s^{-1}$). In addition, hydrogen peroxide may also react with chloride ion under present conditions yielding HOCl (B14). Despite the bulk alkaline pH (Figure 11.4a), the near-surface region (i.e., within electrical double layer) of the metal-doped TiO_2 anode should have a lower pH due to the presence of surface-bound Lewis acid metals, driving reaction B14 and subsequent reaction of H_2O_2 and HClO (B15) to yield O_2.

Primary Electrochemical Oxidant

Most studies of the electrochemical degradation of phenolic compounds with NaCl argue that the primary oxidant is HClO/ClO^-[9,10,12,18,24], which has been reported to chlorinate phenol[42,43]. In contrast, we argue that $Cl_2^{\bullet-}$ is the primary oxidant and that HClO/ClO^- plays a only minor role, if any, in the overall oxidation mechanism. $Cl_2^{\bullet-}$ has a greater one-electron oxidation potential than HClO/ClO^- by 0.5/1.0 eV, and its reaction rate constants with organics are approximately five orders of magnitude greater. In addition, the relative bimolecular rate constants of $Cl_2^{\bullet-}$ with various substrates correlate well with the observed reaction kinetics (Figure 11.5d). On the other hand there is no correlation between relative HOCl rate constants and the observed kinetics (Figure 11.5c). Additionally, $Cl_2^{\bullet-}$ consumption during substrate oxidation (C5a) will inhibit HOCl production (B7, B8) consistent with experimental results.

NaCl electrolysis without substrate produces active chlorine species at the anode, which can be reduced at the cathode (Scheme 11.1) yielding a null chemical cycle. Thus, the chlorine species act as an electron relay between the anode and the cathode, ultimately limiting H_2 production rates. Upon substrate addition during electrolysis at a constant cell voltage (E_{cell}) the active chlorine species rapidly oxidizes the substrates, inhibiting the electron-shuttle pathway consistent with the observed decrease in I_{cell}. Despite the lower I_{cell}, H_2 production increases because a greater fraction of the cathodic electrons are available for H_2O/H^+ reduction, as they are no longer scavenged by active chlorine. If the substrates are not oxidized by the chlorine species, hydrogen production is not enhanced. This argument explains why the extent of synergism is substrate-specific

and dependent upon the substrate oxidation kinetics (i.e., depletion of active chlorine electron scavengers).

For example, the substitution-dependent trend of the observed pseudo-first-order rates in sodium chloride is $-k_{obs}^{PhOH} > -k_{obs}^{2\text{-}CP} > -k_{obs}^{4\text{-}CP} \sim -k_{obs}^{CC} > -k_{obs}^{SA} >> -k_{obs}^{BA}$, which parallels the apparent order of synergistic effects (i.e., ΔEE), PhOH > 2-CP > 4-CP > SA > CC >> BA. Figure 11.7 shows the linear correlations of $-k_{obs}$ vs. $-\Delta I_{cell}$ and $-k_{obs}$ vs. ΔEE with R^2 = 0.90 and 0.91, respectively. This indicates that the substrate oxidation kinetics significantly influences the cathodic hydrogen production. The minimal synergism observed for catechol, in spite of relatively fast electrolytic degradation, can be attributed to a different reaction mechanism. Due to neighboring aromatic -OH groups, catechol adsorbs strongly to the metal oxide surface. Catechol oxidation is likely due to direct electron transfer of the adsorbed (i.e., chelated) catechol to a hole at the anode surface. If the chloride radical anion is, in fact, the primary active chlorine species, then the substrate-dependent reaction rate can be readily interpreted. For example, $-k_{obs}^{HQ}$ is 4.5 times higher than $-k_{obs}^{PhOH}$ and $k_{Cl_2^{\bullet-}+HQ}$ is 5.6 times higher than $k_{Cl_2^{\bullet-}+PhOH}$, while $-k_{obs}^{SA} / -k_{obs}^{PhOH}$ is 0.41 and $k_{Cl_2^{\bullet-}+SA} / k_{Cl_2^{\bullet-}+PhOH}$ is 0.44. The slow reaction rate of $Cl_2^{\bullet-}$ with aliphatic substrates is consistent with the lack of synergy.

Effects of Variable Reaction Parameters

An increase in the concentration of the active chlorine species should affect the electrolytic degradation rates and, subsequently, the rates of hydrogen production at the cathode. When the sodium chloride concentration was increased from 0 to 50 mM in a background sodium sulfate electrolyte (50 mM), $-k_{obs}^{PhOH}$ was observed to increase

linearly (Figure 11.8a). Since $-k_{obs}^{S}$ is the product of the true first-order rate constant ($k_{Cl_2^{\bullet-}+S}$) and the concentration of the reactive chlorine species ($N_{Cl2\bullet-ss}$) which can be varied experimentally, the intrinsic contribution of the active chlorine species to the degradation of phenol, α, can be estimated simply by plotting $-k_{obs}^{S}$ vs. [NaCl].

$$\frac{d[S]}{dt} = -k_{obs}^{S} \times [S] = k_{Cl_2^{\bullet-}+S} \times N_{Cl_2^{\bullet-}} \times [S] \quad (11.6)$$

$$-k_{obs}^{S} = k_{Cl_2^{\bullet-}+S} \times N_{Cl_2^{\bullet-}} = \alpha[NaCl] \quad (11.7)$$

$$\frac{-k_{obs}^{S}}{[NaCl]} = \alpha \quad (11.8)$$

α is determined to be 1.8 M^{-1} min^{-1} with a $R^2 > 0.99$ at 1 mM phenol, 50 mM Na_2SO_4, and I_{cell} = 14.7 mA cm^{-2}. However, when oxidation rates of 50 mM NaCl + 50 mM Na_2SO_4 are compared to 50 mM NaCl (without Na_2SO_4), the latter is found to be higher than the former by a factor of two. This indicates that when present together, the two electrolytes compete for anodic oxidation, and as a consequence, the steady-state concentration of active chlorine radical species are reduced.

The sodium chloride concentration is observed to play a negative role on cathodic hydrogen production, even when present with Na_2SO_4. For example, the current efficiency for the hydrogen production is optimized at 96% under 50 mM Na_2SO_4, decreases to 80% under 50 mM NaCl + 50 mM Na_2SO_4, and is further lowered to 73% under 50 mM NaCl. This observation further confirms that active chlorine radical species act as an electron-shuttle between the anode and the cathode, whereas the primary oxidized sulfate species is not an effective electron shuttle. Therefore, electrolytic production of active chlorine species from chloride has a negative effect on the net

cathodic process of H_2 production relative to sulfate, but a positive effect on the anodic substrate oxidation.

In addition to the concentration of the supporting electrolyte, the applied cell current also directly affects the efficiencies of the hybrid reactions. $-k_{obs}^{S}$ is linearly correlated to I_{cell} with a slope of 12.6 $min^{-1}A^{-1}cm^2$ ($R^2 > 0.98$). As a consequence, the reaction of 1 mM phenol at I_{cell} values up to 40 mA cm^{-2} is in the reaction-limited regime. In this regime, the overall reaction rate is limited by the low steady-state concentration of aqueous oxidizing radicals within the dynamic reaction zone. Thus, less-active chlorine species are produced at the anode than are required to oxidize all of the substrate molecules that enter the reaction zone. The pseudo-first-order kinetics is representative of competition between the initial substrate and its intermediates for oxidizing radicals. The number of dichloride radical anions can be estimated in this regime (eq. 11.9).

$$N_{Cl_2^{\bullet-}} = \frac{-k_{obs}^{S}}{k_{Cl_2^{\bullet-}+S}} \tag{11.9}$$

At a I_{cell} = 14.7 mA/cm^2, ($[Cl_2^{\bullet-}]_{ss}$ is calculated to be 1.4×10^{-11} mol L^{-1}). This value is three orders of magnitude greater than the number of hydroxyl radicals estimated from eq. 11.5, but still many orders of magnitude lower than typical substrate concentration, [S]. In contrast, the cathodic hydrogen production rate does not correlate linearly with the I_{cell}; rather, its current efficiency increases from 45% at 7 mA cm^{-2} to 67% at 14.7 mA cm^{-2}, and then levels off at higher I_{cell}.[8] As the I_{cell} value increases, more H_2 is produced. However, the H_2 current efficiency decreases due to increasing number of dichloride radical anions that are produced, which can scavenge electrons.

In a sodium sulfate electrolyte system, analogous to the chloride system, a one-electron oxidation of sulfate to the sulfate radical ($SO_4^{\bullet-}$) is predicted to produce the primary reactive species (eq. 11.10). In spite of the high redox potential of the sulfate radical, the substrate oxidation rates are two orders of magnitude lower than observed with sodium chloride. This is at variance with expectations from previously reported $SO_4^{\bullet-}$ oxidation kinetics (i.e, $k_{SO_4^{\bullet-}+Ar} / k_{Cl_2^{\bullet-}+Ar}$ = 10 - 100).[36] Thus, if free $SO_4^{\bullet-}$ was produced, phenol degradation in Na_2SO_4 would be faster than in NaCl, suggesting that if $SO_4^{\bullet-}$ is produced, it is strongly bound to the metal oxide surface. Surface-bound $SO_4^{\bullet-}$ may react with another surface-bound $SO_4^{\bullet-}$ to produce persulfate, $S_2O_8^{2-}$ (eq. 11.11) or surface-bound $SO_4^{\bullet-}$ may react with surface-bound $^{\bullet}OH$ to produce peroxymonosulfate, SO_5H^-. As non-radical species that would require a two-electron reduction, $S_2O_8^{2-}$ would scavenge cathodic electrons at a much slower rate than $Cl_2^{\bullet-}$. Persulfate can be homolytically cleaved into two sulfate radicals photolytically or thermally[44,45]. but is stable under ambient conditions. Persulfate can be transformed into two sulfate anions and oxygen (eq 11.12) or a peroxymonosulfate and sulfate (eq 11.13). Peroxymonosulfate can be transformed into hydrogen peroxide and sulfate (eq 11.14).

$$> \text{Ti-OH}^{\bullet} + SO_4^{2-} \rightarrow > \text{Ti-OH}\,(e^-) + SO_4^{\bullet-} \qquad (11.10)$$

$$SO_4^{\bullet-} + SO_4^{\bullet-} \rightarrow S_2O_8^{2-} \qquad (11.11)$$

$$S_2O_8^{2-} + H_2O \rightarrow 2SO_4^{2-} + 2H^+ + 0.5O_2 \qquad (11.12)$$

$$S_2O_8^{2-} + H_2O \rightarrow SO_5^{2-} + SO_4^{2-} + 2H^+ \qquad (11.13)$$

$$SO_5^{2-} + H_2O \rightarrow H_2O_2 + SO_4^{2-} \qquad (11.14)$$

Figures

Figure 11.1. H_2, O_2, and CO_2 production during phenol electrolysis. E_{cell} = 3.1 V. The BiO_x-TiO_2-Ti anode and stainless-steel cathode couple was immersed in 50 mM NaCl (0.2 L) where N_2 was continuously purged through solution. 1.0 mM phenol was spiked at intervals into the solution (as indicated by arrows). The system control was H_2 production via pure water electrolysis without addition of phenol.

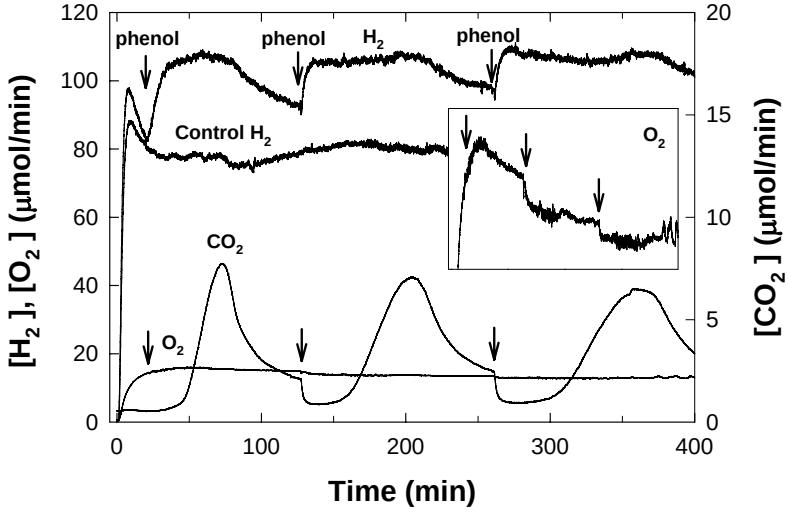

Figure 11.2. A) Effect of various substrate additions on the H_2 production rate. Constant E_{cell}s in 50 mM NaCl solution. See Table 11.1 for E_{cell}s. The sidebars refer to hydrogen production rates of 5×10^{-6} mol/min. B) Time profiles of the electrolytic degradation of substrates (1 mM) at I_{cell} = 0.375 A in 50 mM sodium chloride solution. See Table 11.1 for more information.

A

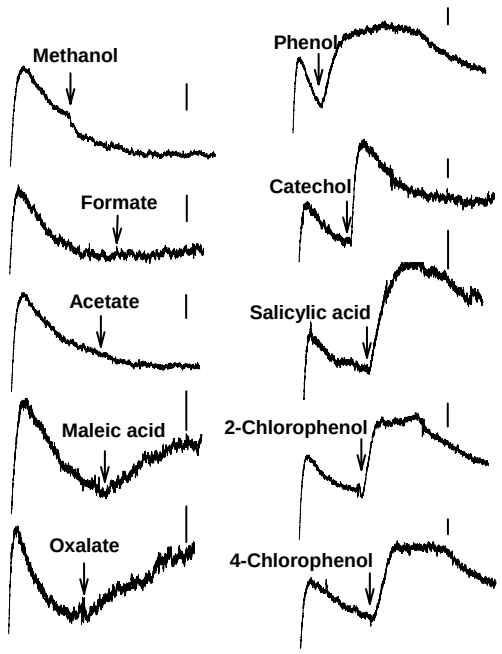

B

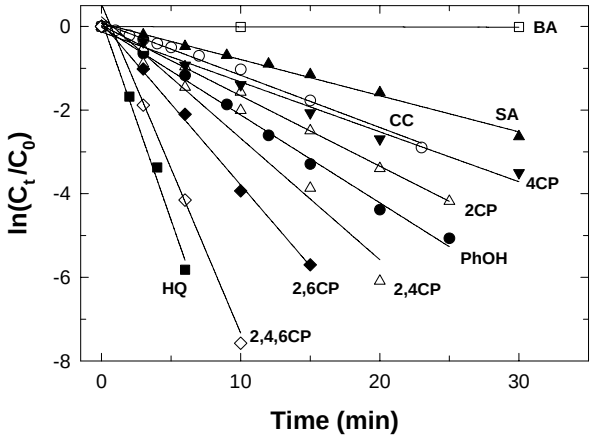

Figure 11.3. Effect of electrolyte, NaCl vs. Na_2SO_4, on electrochemical processes. A) Energy efficiencies for the electrolytic hydrogen production as a function of applied cell power in 50 mM sodium sulfate or 50 mM sodium chloride. B) Effect of 1 mM phenol addition on the electrolytic hydrogen production in 50 mM sodium sulfate. E_{cell} = 3.04 V. C) Time profiles of the electrolytic degradation of substrates (~ 1 mM) in 50 mM sodium sulfate at I_{cell} = 0.375 A. (The NaCl data in (a) is taken from reference 8 for comparison.)

A

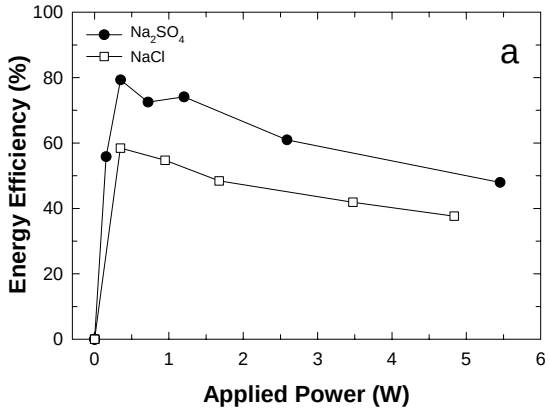

B

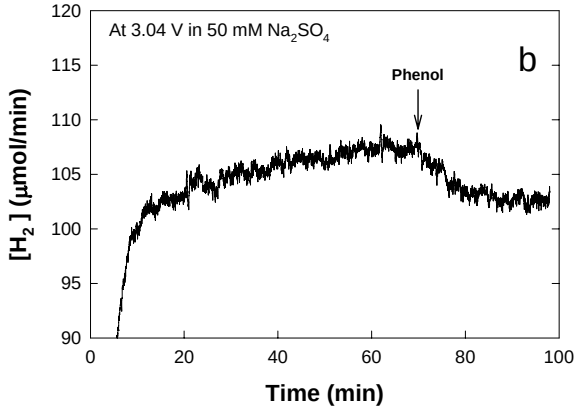

C

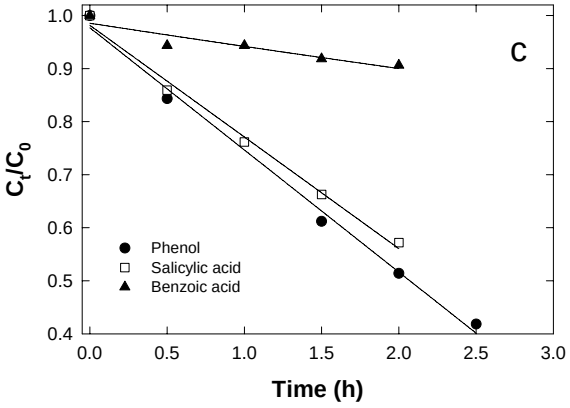

Figure 11.4. Time profiles of pH variation during electrolysis with and without phenol. $[Phenol]_0$ = 1 mM A) in 50 mM sodium chloride and B) in 50 mM sodium sulfate. I_{cell} = 0.375 A. (Figure (A) is taken from reference 8 for comparison.)

A

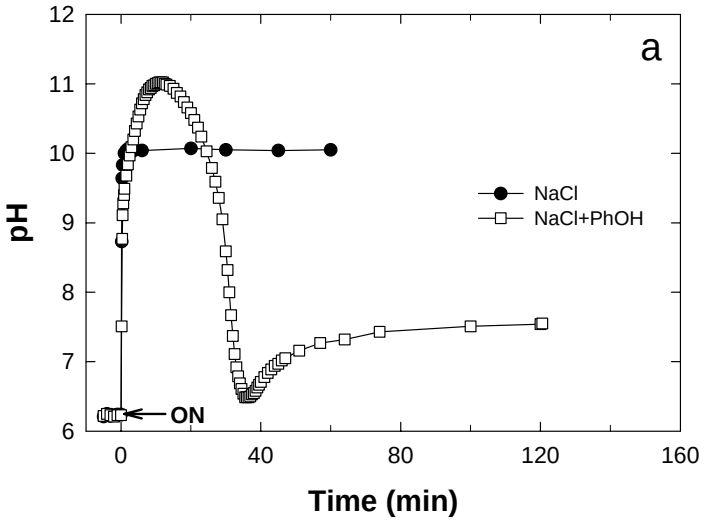

B

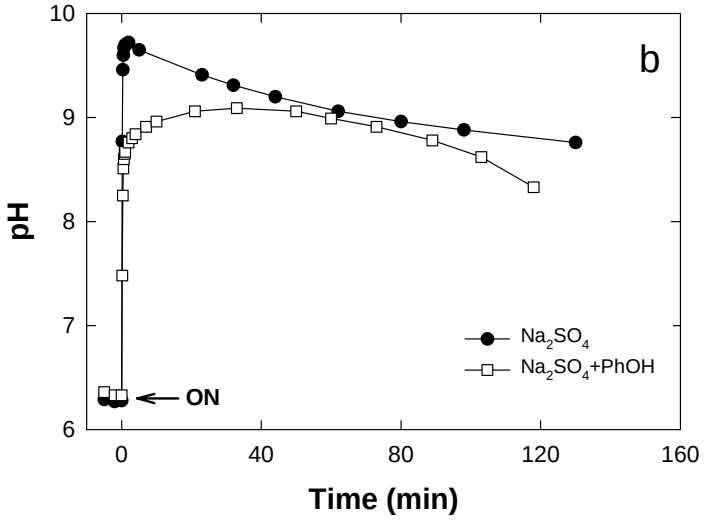

Figure 11.5. Relationships between k^0_{obs}, k^0_{OH}, $k^0_{Cl_2^{\bullet-}}$, k^0_{HClO}. A) k^0_{obs} vs. k^0_{OH}. B) k^0_{obs} vs. $k^0_{Cl_2^{\bullet-}}$ C) k^0_{obs} vs. k^0_{HClO}, and D) Hammett constant vs. k^0_{obs}. See Table 11.1 and text for more detailed information

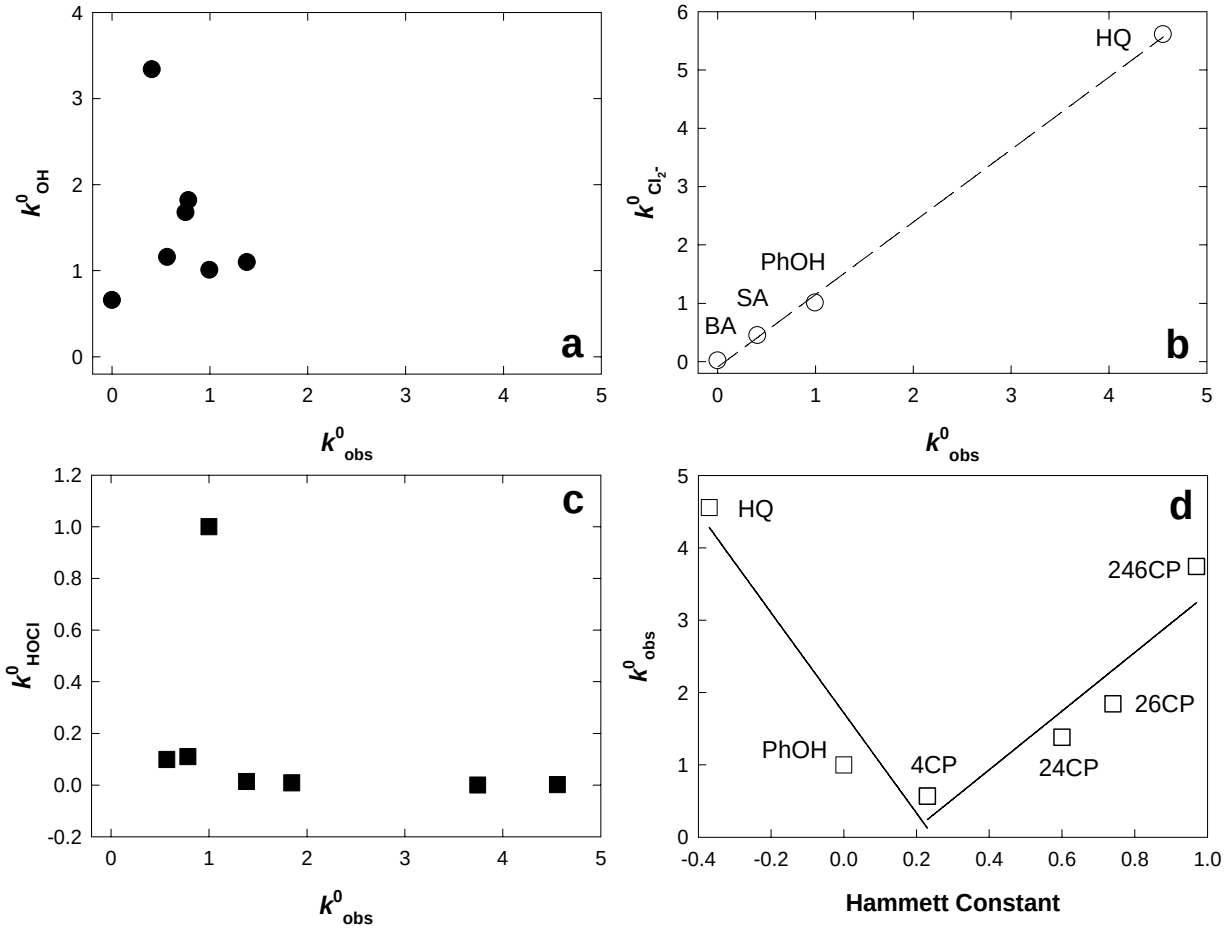

Figure 11.6. Hypochlorite production during electrolysis. A) [NaCl] = 50 mM. The inset shows the UV-vis absorption spectrum of the produced hypochlorite. I_{cell} = 0.375 A. B) Effects of spiking 5 mM sodium hypochlorite on the hydrogen and oxygen production, and on the change of I_{cell}. E_{cell} = 3.17 V. [NaCl] = 50 mM

A

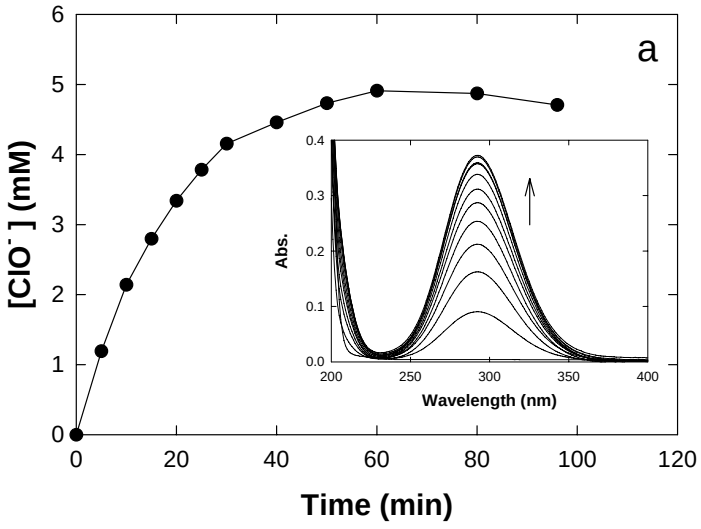

B

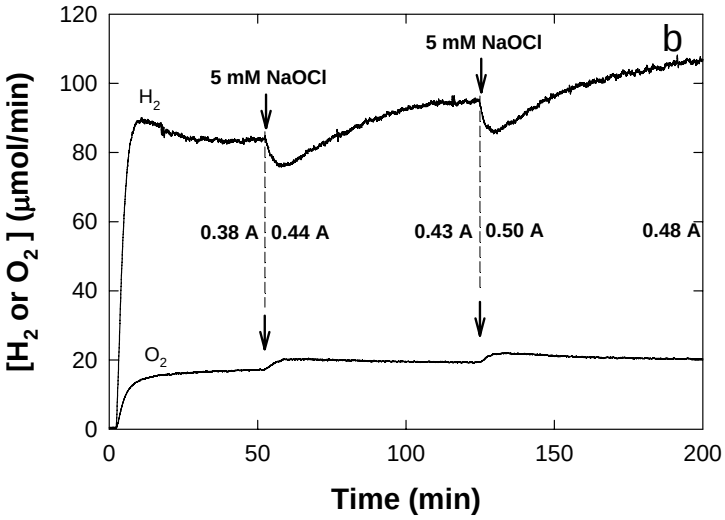

Figure 11.7. Electrochemical relationships of $-k_{obs}$ vs. ΔI_{cell} and $-k_{obs}$ vs. ΔEE. (See Table 11.1 and the text for more detailed information.)

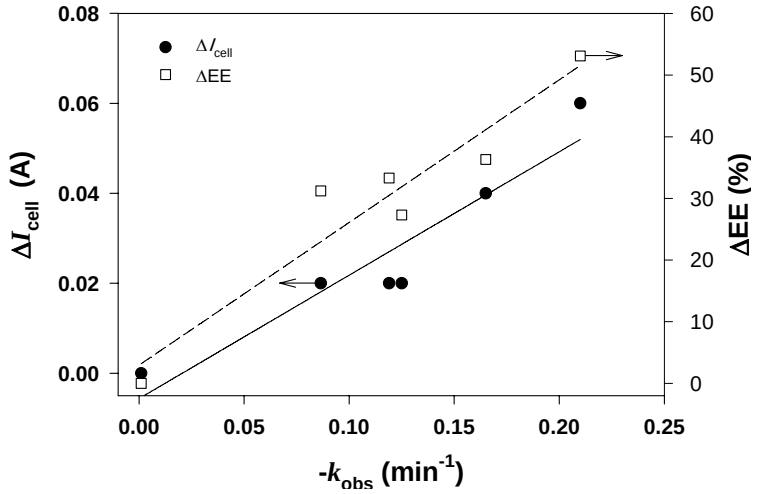

Figure 11.8. $-k_{obs}$ and I_{cell} vs. NaCl concentration in 50 mM Na_2SO_4. A) the electrolytic degradation rates of 1 mM phenol and on B) the current efficiencies for the hydrogen production. I_{cell} = 0.375 A; [Na_2SO_4] = 50 mM. NaCl only refers to 50 mM NaCl without Na_2SO_4. The numbers in insets refer to [NaCl] (mM)

A

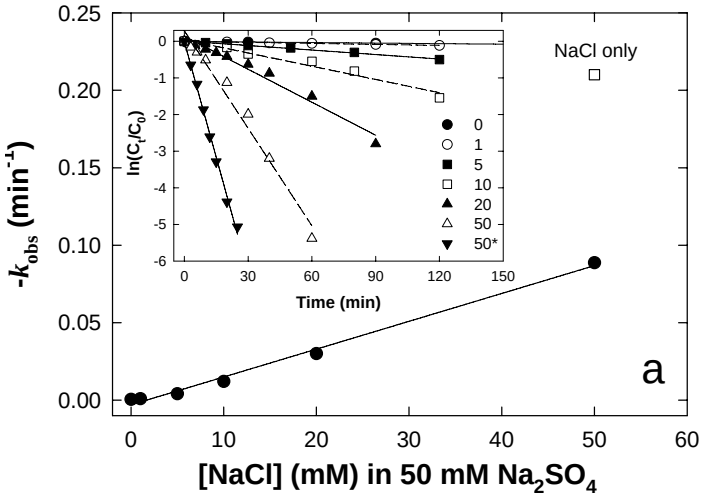

B

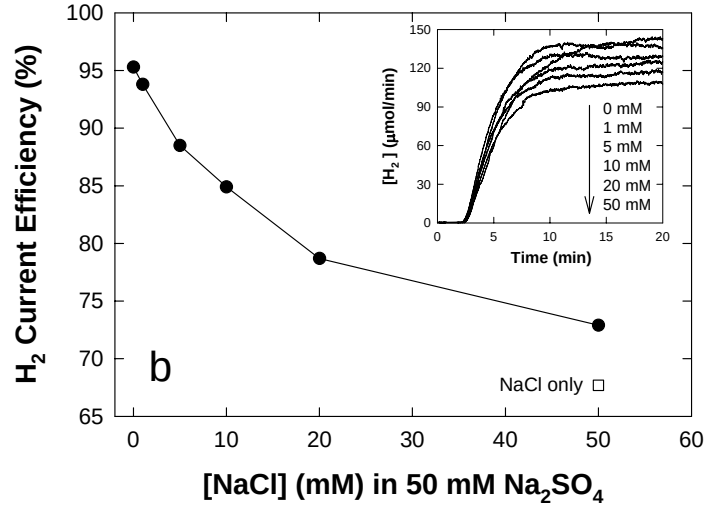

Figure 11.9. Effect of applied cell current (I) on $-k_{obs}$ of phenol. [NaCl] = 50 mM

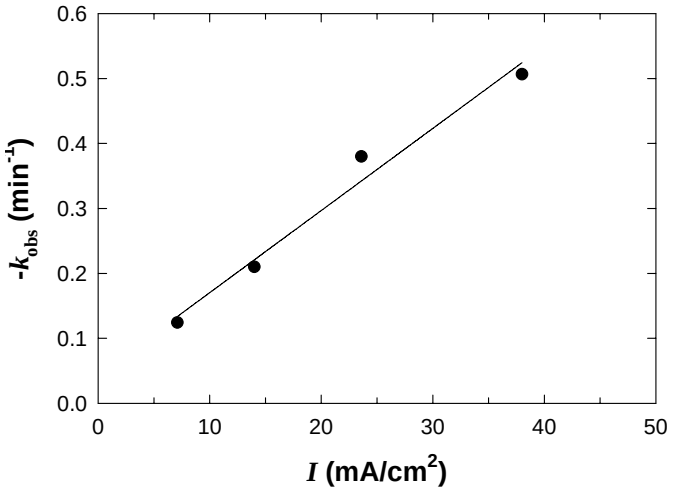

Schemes

Scheme 11.1. Representation of electrochemical reaction network

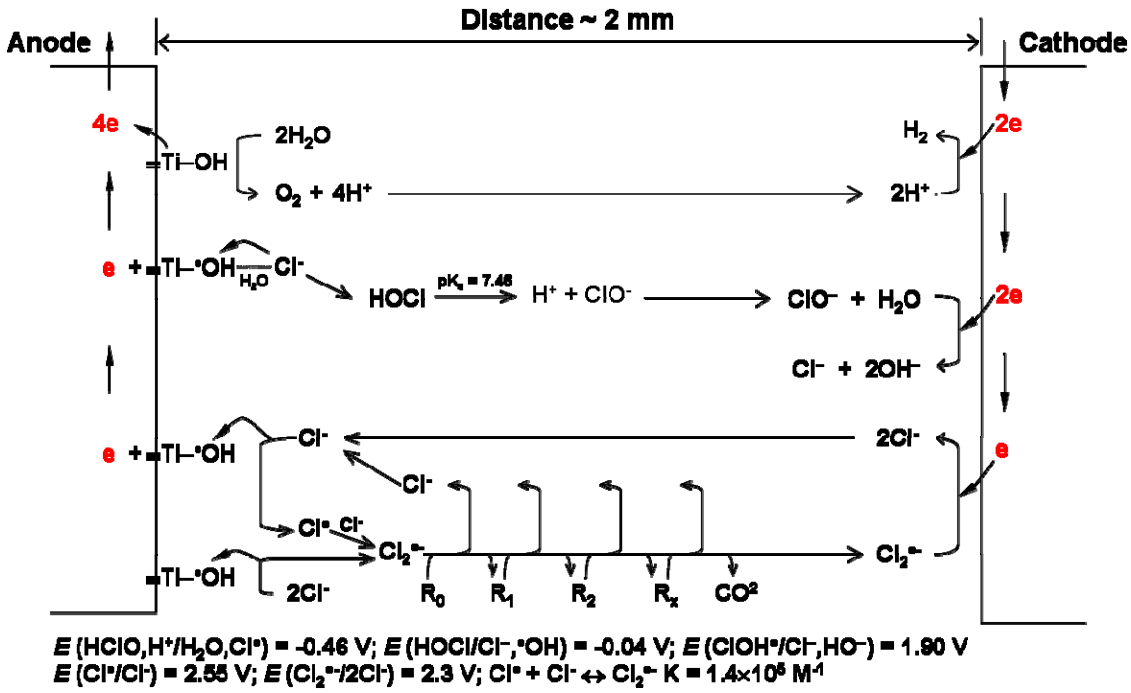

Tables

Table 11.1. Electrochemical reaction rates and properties of the substrates

Substrate	$-k^{S}_{obs}$ (min^{-1})[b] in NaCl	$-k^{S}_{obs}$ (min^{-1})[b] in Na_2SO_4	k_{OH+S} ($M^{-1}s^{-1}$)[e]	$k_{Cl\bullet+S}$ ($M^{-1}s^{-1}$)[f]	$k_{Cl_2^{\bullet-}+S}$ ($M^{-1}s^{-1}$)[f]	k_{HOCl+S} ($M^{-1}s^{-1}$)[g]	$E_{1/2}$ (V_{SCE})[h]	pK_a	E_{cell} (V)[i]	ΔH_2 (μmol /min)[i]	ΔI_{cell} (A)[i]	ΔEE (%)[i]
Methanol			9.7×10^{8}		3.5×10^{3}			15.5	3.10	0	0	0
Formate			3.2×10^{9}	1.3×10^{8}	1.9×10^{6}				3.15	0	0	0
Formic acid			1.3×10^{8}		6.7×10^{3}			3.75				
Acetate			8.5×10^{7}						3.10	0	0	0
Acetic acid			1.6×10^{7}	2.0×10^{8}	$< 1\times10^{4}$			4.76				
Maleic acid			6.0×10^{9}						3.07	+5	0	8.0
Malonic acid			1.6×10^{7}									
Oxalate			7.7×10^{6}						3.05	+7	0	10.2
Oxalic acid			1.4×10^{6}									
PhOH[a]	[c]0.210 (*1*)[d]	[c]5.64×10^{-3} (*1*)	6.6×10^{9} (*1*)	2.5×10^{10}	2.5×10^{8} (*1*)	2.19×10^{4} (*1*)	0.633	9.95	3.10	+20	–0.06	53.1
CC	0.125 (*0.59*)		1.1×10^{10} (*1.67*)				0.507	9.85	3.25	+22	–0.02	27.3
HQ	0.957 (4.55)		5.2×10^{9} (*0.79*)		1.4×10^{9} (*5.6*)	4.5×10^{1} (*2.1×10^{-3}*)	0.507	9.96				
2CP	0.165 (*0.78*)		1.2×10^{10} (*1.81*)			2.42×10^{3} (*0.11*)	0.625	8.29	3.14	+14	–0.04	36.3
4CP	0.119 (*0.57*)		7.6×10^{9} (*1.15*)			2.17×10^{3} (*0.10*)	0.653	9.14	3.18	+20	–0.02	33.3
24CP	0.290 (*1.38*)		7.2×10^{9} (*1.09*)			3.03×10^{2} (*0.014*)	0.645	8.09				
26CP	0.388 (*1.84*)					1.94×10^{2} (*8.9×10^{-3}*)		6.8				
246CP	0.787 (*3.74*)		5.4×10^{9} (*0.82*)			1.28×10^{1} (*5.8×10^{-4}*)	0.637	6.21				
SA	0.0865 (*0.41*)	4.59×10^{-3} (*0.81*)	2.2×10^{10} (*3.33*)		1.1×10^{8} (*0.44*)		0.845 (pH 13)	2.97	3.17	+12	–0.02	31.2
BA	1×10^{-3} (*0.0045*)	7.55×10^{-4} (*0.13*)	4.3×10^{9} (*0.65*)		2×10^{6} (*0.008*)			4.20	3.15	0	0	0

a. PhOH: phenol, CC: catechol, HQ: hydroquinone, 2CP: 2-chlorophenol, 4CP: 4-chlorophenol, 24CP: 2,4-dichlorophenol, 26CP: 2,6-dichlorophenol, 246CP: 2,4,6-trichlorophenol, SA: salicylic acid (2-hydroxy benzoic acid), BA: benzoic acid.
b. The observed pseudo-first order reaction rates of substrates in 50 mM NaCl or 50 mM Na_2SO_4.
c. Concentrations of substrates, $1 \sim 2\times10^{-3}$ M; I_{cell} = 0.375 A in 50 mM NaCl or 50 mM Na_2SO_4.
d. The numbers in parenthesis are the reaction rates of the substrate with respect to phenol.
e. See ref. 27
f. See ref. 28 and 29.
g. See ref. 39.

h. Half wave potential measured at pH 5.6 in 50% aqueous isopropyl alcohol unless noted otherwise. For more information see ref 31.
i. At constant cell potential (E_{cell}) a corresponding substrate was added, and then the consequent difference of hydrogen production rate (ΔH_2 = rate after addition – rate before addition), cell current (ΔI_{cell} = current after addition – current before addition), and energy efficiency (ΔEE = (EE after addition – EE before addition) / EE before addition × 100%) were measured and calculated.

Table 11.2. Elementary electrochemical reaction steps

Entry	Reaction	Value
	Reaction Initiation and Generation of Reactive Species	
A1-a	$>\text{Ti-OH} \rightarrow >\text{Ti-OH}^{\bullet} + e^-$	I_{an}^{OH}
A1-b	$\equiv \text{Ti-OH}^{\bullet} + H_2O \rightarrow \equiv \text{Ti-OH} + OH^{\bullet} + H^+ + e^-$	I_{an}^{OH}
A2	$\equiv \text{Ti-OH}^{\bullet} + 0.5H_2O \rightarrow \equiv \text{Ti-OH} + 0.25O_2 + H^+ + e^-$	$I_{an}^{O_2}$, k_{O_2}
A3	$\equiv \text{Ti-OH}^{\bullet} + 0.5H_2O + 0.25O_2 \rightarrow \equiv \text{Ti-OH} + 0.5H_2O_2$	$k_{H_2O_2}$
A4-a	$\equiv \text{Ti-OH}^{\bullet} + Cl^- \rightarrow \equiv \text{Ti-OHCl}^{\bullet-}$	k_{OHCl}
A4-b	$\equiv \text{Ti-OHCl}^{\bullet-} + H_2O + H^+ \rightarrow \equiv \text{Ti-OH} + 2H_2O + Cl^{\bullet}$	$k_{OH,Cl}$
A5	$\equiv \text{Ti-OH}^{\bullet} + Cl^- + H_2O \rightarrow \equiv \text{Ti-OH} + HOCl + H^+ + e^-$	
A6	$\equiv \text{Ti-OH}^{\bullet} + R_n \rightarrow \equiv \text{Ti-OH} + R_n^{\bullet}$	$k_{Rn,OH}$
A7-a	$O_2 + e^- \rightarrow O_2^{\bullet-}$	E = – 0.33 V
A7-b	$O_2^{\bullet-} + H^+ \rightarrow HOO^{\bullet}$	$pK_a = 4.88$
A7-c	$2HOO^{\bullet} \rightarrow H_2O_2 + O_2$	
	Reactions of Reactive Species (no distinction between >Ti-OH$^{\bullet}$ and OH$^{\bullet}$)	
B1	$OH^{\bullet} + Cl^- \rightleftharpoons ClOH^{\bullet-}$	K = 0.70
B2	$ClOH^{\bullet-} + H^+ \rightleftharpoons Cl^{\bullet} + H_2O$	$K = 1.6\times10^7$
B3	$Cl^{\bullet} + Cl^{\bullet} \rightarrow Cl_2$	k_{2Cl}
B4a	$Cl^{\bullet} + Cl^- \rightarrow Cl_2^{\bullet-}$	$k = 8.5\times10^9\ M^{-1}\ s^{-1}$
B4b	$Cl_2^{\bullet-} \rightarrow Cl^{\bullet} + Cl^-$	$k = 6.0\times10^4\ s^{-1}$
B5	$Cl^{\bullet} + Cl_2^{\bullet-} \rightarrow Cl^- + Cl_2$	$k = 1.4\times10^9\ M^{-1}\ s^{-1}$
B6	$Cl_2^{\bullet-} + Cl_2^{\bullet-} \rightarrow 2Cl^- + Cl_2$	$k = 3.5\times10^9\ M^{-1}\ s^{-1}$
B7	$Cl_2^{\bullet-} + H_2O \rightarrow HOCl + Cl^- + H^+ + e^-$	$k[H_2O] < 1300\ s^{-1}$
B8	$Cl_2^{\bullet-} + OH^{\bullet} \rightarrow HOCl + Cl^-$	
B9	$OH^{\bullet} + OH^{\bullet} \rightarrow H_2O_2$	
B10	$H_2O_2 + OH^{\bullet} \rightarrow HOO^{\bullet} + H_2O$	$k = 3.2\times10^7\ M^{-1}\ s^{-1}$
B11	$H_2O_2 + Cl^{\bullet} \rightarrow HOO^{\bullet} + H^+ + Cl^-$	$k = 2.0\times10^9\ M^{-1}\ s^{-1}$
B12	$H_2O_2 + Cl_2^{\bullet-} \rightarrow HOO^{\bullet} + H^+ + 2Cl^-$	$k = 1.4\times10^5\ M^{-1}\ s^{-1}$
B13	$HOO^{\bullet} + Cl_2^{\bullet-} \rightarrow O_2 + H^+ + 2Cl^-$	$k = 3.1\times10^9\ M^{-1}\ s^{-1}$

B14	$H_2O_2 + Cl^- + H^+ \rightarrow HClO + H_2O$	
B15	$H_2O_2 + HClO \rightarrow H_2O + O_2 + H^+ + Cl^-$	
B16	$HClO \rightleftharpoons H^+ + ClO^-$	$pK_a = 7.46$
B17	$HClO + H^+ \rightleftharpoons Cl^+ + H_2O \rightleftharpoons H_2ClO^+$	
B18	$2HClO + H^+ \rightarrow Cl_2O + H^+ + H_2O$	
B19	$HClO + H^+ + Cl^- \rightarrow Cl_2 + H_2O$	
B20	$HClO + 0.5H_2O \rightarrow 1/3ClO_3^- + 2/3Cl^- + 2H^+ + 0.25O_2 + e^-$	

Reactions of Reactive Species with Substrates

C1	$OH^\bullet$ + H-Ph-OH $\rightarrow\rightarrow$ Degradation products	
C2	H_2O_2 + H-Ph-OH $\rightarrow\rightarrow$ Degradation products	
C3	HClO + PhOH $\rightarrow\rightarrow$ Degradation products	
C4	$Cl^\bullet$ + H-Ph-OH $\rightarrow\rightarrow$ Degradation products	
C5-a	$Cl_2^{\bullet-}$ + H-Ph-OH $\rightarrow$ H-$Ph^{\bullet+}$-OH + $2Cl^-$	
C5-b	H-$Ph^{\bullet+}$-OH + $H_2O \rightleftharpoons$ H-Ph-$O^\bullet$ + H^+	$pK_a = -2.0$
C5-c	H-Ph-$O^\bullet$ + $Cl_2^{\bullet-} \rightarrow$ Cl-Ph-OH + Cl^-	
C5-d	Cl-Ph-OH + $Cl_2^{\bullet-} \rightarrow\rightarrow$ Degradation products	

Annihilation of Reactive Species

D1	$Cl^\bullet + e^- \rightarrow Cl^-$	E = 2.4 V
D2	$Cl_2^{\bullet-} + e^- \rightarrow 2Cl^-$	E = 2.0 V
D3a	$HClO + H^+ + e^- \rightarrow 0.5Cl_2 + H_2O$	E = 1.63 V
D3b	$HClO + H^+ + 2e^- \rightarrow Cl^- + H_2O$	E = 1.49 V
D3a	$ClO^- + 2e^- + H_2O \rightarrow Cl^- + 2OH^-$	E = 0.90 V

Cathodic Hydrogen and Oxygen Production

E1	$O_2 + 4H^+ + 4e^- \rightarrow 2H_2O$	E = 1.23 V
E2	$H_2O + e^- \rightarrow 0.5H_2 + OH^-$	E = - 0.83 V

References

(1) *International Energy Outlook 2006*; Energy Information Administration.

(2) Penner, S. S. *Energy* **2006**, *31*, 33.

(3) *Solar and Wind Technologies for Hydrogen Production*, available at http://www.hydrogen.energy.gov/congress_reports.html.

(4) Ivy, J. *Summary of Electrolytic Hydrogen Production: Milestone Completion Report*, available at www.nrel.gov/hydrogen/pdfs/36734.pdf.

(5) Kroposki, B.; Levene, J.; Harrison, K.; P.K., S.; Novachek, F. *Electrolysis: Information and opportunities for electric power utilities*, available at http://www.osti.gov/bridge.

(6) *Water and Wastewater Industry Energy Efficiency: A Research Roadmap*, available at http://www.energy.ca.gov/2004publications/CEC.

(7) Park, H.; Vecitis, C. D.; Choi, W.; Weres, O.; Hoffmann, M. R. *J. Phys. Chem. C* **2008**, *112*, 885.

(8) Park, H.; Vecitis, C. D.; Hoffmann, M. R. *J. Phys. Chem. A* **2008**, *112*, 7616.

(9) Weres, O. *National Science Foundation Phase I Final Report (SRC-020)* **1995**.

(10) Comninellis, C.; Nerini, A. *J. Appl. Electrochem.* **1995**, *25*, 23.

(11) Lin, S. H.; Shyu, C. T.; Sun, M. C. *Water Res.* **1998**, *32*, 1059.

(12) Bonfatti, F.; Ferro, S.; Lavezzo, F.; Malacarne, M.; Lodi, G.; De Battisti, A. *J. Electrochem. Soc.* **2000**, *147*, 592.

(13) Korbahti, B. K.; Salih, B.; Tanyolac, A. *J. Chem. Technol. Biotechnol.* **2002**, *77*, 70.

(14) Wang, J. K.; Farrell, J. *Environ. Sci. Technol.* **2004**, *38*, 5232.

(15) Fino, D.; Jara, C.; Saracco, G.; Specchia, V.; Spinelli, P. *J. Appl. Electrochem.* **2005**, *35*, 405.

(16) Rajkumar, D.; Kim, J. G.; Palanivelu, K. *Chem. Eng. Technol.* **2005**, *28*, 98.

(17) Bonfatti, F.; De Battisti, A.; Ferro, S.; Lodi, G.; Osti, S. *Electrochim. Acta* **2000**, *46*, 305.

(18) Martinez-Huitle, C. A.; Ferro, S.; De Battisti, A. *Electrochem. Solid State Lett.* **2005**, *8*, D35.

(19) Nikolaevsky, R.; Monosov, M.; Monosov, E.; Sharony, E.; Gurevich, D. *Method for Purification of Wastewater from Soluble Substances;* U.S. Patent 5,792,336; Aug. 11, **1998**.

(20) Zhan, X. M.; Wang, J. L.; Wen, X. H.; Qian, Y. *Environ. Technol.* **2001**, *22*, 1105.

(21) Naumczyk, J.; Szpyrkowicz, L.; ZilioGrandi, F. *Water Sci. Technol.* **1996**, *34*, 17.

(22) Weres, O. *Electrode with Surface Comprising Oxides of Titanium and Bismuth and Water Purification Process Using This Electrode,* U.S. Patent 0,000,774 A1, Jan. 4, **2007**.

(23) Murugananthan, M.; Yoshihara, S.; Rakuma, T.; Uehara, N.; Shirakashi, T. *Electrochim. Acta* **2007**, *52*, 3242.

(24) Kaba, L.; Hitchens, G. D.; Bockris, J. O. *J. Electrochem. Soc.* **1990**, *137*, 1341.

(25) Zhu, X.; Shi, S.; J, W.; Lu, F.; Zhao, H.; Kong, J.; He, Q.; Ni, J. *Environ. Sci. Technol.* **2007**, *41*, 6541.

(26) Torres, R. A.; Torres, W.; Peringer, P.; Pulgarin, C. *Chemosphere* **2003**, *50*, 97.

(27) Buxton, G. V.; Greenstock, C. L.; Helman, W. P.; Ross, A. B. *J. Phys. Chem. Ref. Data* **1988**, *17*, 513.

(28) Yu, X. Y. *J. Phys. Chem. Ref. Data* **2004**, *33*, 747.

(29) Neta, P.; Huie, R. E.; Ross, A. B. *J. Phys. Chem. Ref. Data* **1988**, *17*, 1027.

(30) Kesselman, J. M.; Weres, O.; Lewis, N. S.; Hoffmann, M. R. *J. Phys. Chem. B* **1997**, *101*, 2637.

(31) Wardman, P. *J. Phys. Chem. Ref. Data* **1989**, *18*, 1637.

(32) Buxton, G. V.; Bydder, M.; Salmon, G. A.; Williams, J. E. *Phys. Chem. Chem. Phys.* **2000**, *2*, 237.

(33) Gilbert, B. C.; Stell, J. K.; Peet, W. J.; Radford, K. J. *J. Chem. Soc.—Faraday Trans. I* **1988**, *84*, 3319.

(34) Buxton, G. V.; Bydder, M.; Salmon, G. A. *J. Chem. Soc.—Faraday Trans.* **1998**, *94*, 653.

(35) Alegre, M. L.; Gerones, M.; Rosso, J. A.; Bertolotti, S. G.; Braun, A. M.; Martire, D. O.; Gonzalez, M. C. *J. Phys. Chem. A* **2000**, *104*, 3117.

(36) Hasegawa, K.; Neta, P. *J. Phys. Chem.* **1978**, *82*, 854.

(37) Padmaja, S.; Neta, P.; Huie, R. E. *J. Phys. Chem.* **1992**, *96*, 3354.

(38) Anslyn, E. V.; Dougherty, D. A. *Modern Physical Organic Chemistry*; University Science Books: Sausalito, CA, **2006**.

(39) Richard, J. P.; Jencks, W. P. *J. Am. Chem. Soc.* **1982**, *104*, 4689.

(40) Gallard, H.; von Gunten, U. *Environ. Sci. Technol.* **2002**, *36*, 884.

(41) Ferro, S.; De Battisti, A.; Duo, I.; Comninellis, C.; Haenni, W.; Perret, A. *J. Electrochem. Soc.* **2000**, *147*, 2614.

(42) Vione, D.; Maurino, V.; Minero, C.; Calza, P.; Pelizzetti, E. *Environ. Sci. Technol.* **2005**, *39*, 5066.

(43) Moye, C. J.; Sternhel, S. *Aust. J. Chem.* **1966**, *19*, 2107.

(44) Hori, H.; Yamamoto, A.; Hayakawa, E.; Taniyasu, S.; Yamashita, N.; Kutsuna, S. *Environ. Sci. Technol.* **2005**, *39*, 2383.

(45) Canizares, P.; Saez, C.; Lobato, J.; Rodrigo, M. A. *Ind. Eng. Chem. Res.* **2004**, *43*, 6629.